Comparison of Langmuir probe and laser Thomson scattering for plasma density and electron temperature measurements in HiPIMS plasma

Peter J. Ryan,[a] James W. Bradley, and Mark D. Bowden
Department of Electrical Engineering and Electronics, University of Liverpool, Brownlow Hill, Liverpool L69 3GJ, United Kingdom

(Dated: 7 May 2019)

The temporal evolution of plasma density and electron temperature in HiPIMS discharges has been measured using the Langmuir probe and laser Thomson scattering techniques. Measurements were performed (non-simultaneously) at two positions within the plasma; in the low magnetic field strength region on the discharge axis and in the high magnetic field strength region of the magnetic trap, for peak power densities of 450 $\mathrm{Wcm^{-2}}$ and 900 $\mathrm{Wcm^{-2}}$ respectively. The maximum plasma densities and temperatures were 6.9×10^{19} $\mathrm{m^{-3}}$ and 3.7 eV in the pulse-on time, and values decayed to 4.5×10^{17} $\mathrm{m^{-3}}$ and 0.1 eV at times up to 250 μs into the afterglow. The results indicate that although intrusive, the Langmuir probe can provide a good indication of electron properties in regions of different electron magnetization in the discharge.

High power impulse magnetron sputtering (HiPIMS) is a novel ionized physical vapour deposition (IPVD) technique[1] in which high metal ionization fractions ($\sim$ 70% in Kouznetsov *et al*[2]) are obtained through the creation of a dense plasma ($\sim 10^{19}$ $\mathrm{m^{-3}}$). This necessitates high target power densities (0.5-10 $\mathrm{kWcm^{-2}}$) and these are generated using short high-voltage pulses (width $\sim 10-100$ μs) with low duty cycle ($\sim$ 1%) to prevent target melting. The main advantage of IPVD is that the energy and directionality of the film forming ions can be controlled by biasing the substrate, in contrast to line of sight deposition using neutrals.[3] This results in HiPIMS producing films with superior properties (e.g. denser, harder and smoother) compared to DC magnetron operation.[4–6]

A schematic of an unbalanced planar magnetron is shown in figure 1. Electrons perform a closed $E\times B$ drift inside the last closed flux surface boundary, which confines electrons and produces a dense plasma. This magnetic trap region produces the most intense ionization in the discharge, predominately through the process of electron impact ionization.[7] There are also open flux surfaces that guide electrons which have escaped the trap (and consequently ions through ambipolar diffusion) from the target vicinity to the substrate position. A detailed understanding of the plasma dynamics inside the magnetic trap and at the substrate is required in order to optimize the deposition process. The most fundamental plasma properties for any physics investigation are electron density (n_e) and temperature (T_e).

Unfortunately HiPIMS poses a difficult environment for diagnostic operation due to the high sputter flux; the relative abundance of species has a dynamic evolution; n_e between pulses spans several orders of magnitude and T_e at least an order of magnitude; and the plasma is spatially heterogeneous. These effects are most pronounced inside the magnetic trap. Non-intrusive diagnostics are obviously desirable and examples of such techniques applied to HiPIMS include optical emission spectroscopy[8–10] and recently THz time-domain

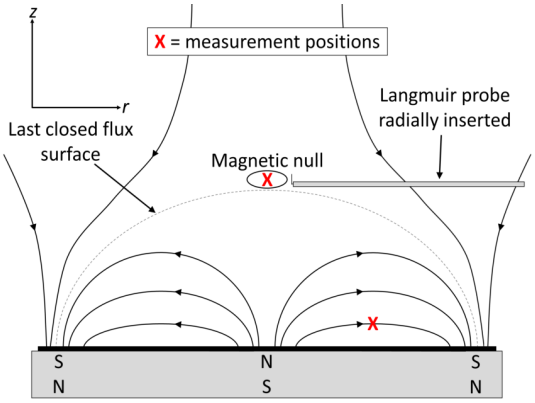

FIG. 1. Schematic of the magnetic field from an unbalanced planar magnetron. In this study the tungsten target diameter was 150 mm and the measurement positions were at the magnetic null ($r=0$ mm, $z=61$ mm) and at a single location inside the last closed flux surface boundary ($r=41$ mm, $z=10$ mm). The system origin ($r=0$ mm, $z=0$ mm) is located at the center of the target surface. For reference, the main racetrack erosion is at ($r=48$ mm, $z=0$ mm).

spectroscopy.[11] The former can be implemented with relative ease to give time-resolved information about the abundance of excited species, but it is challenging to extract quantitative information about electron properties because a complicated model describing electronic transitions is required. The latter is a novel technique for measuring electron density, but it has a relatively high detection limit ($n_e > 10^{18}$ $\mathrm{m^{-3}}$), so measurements during the pulse off time (afterglow) are limited, and it has a long integration time (3 hours). A drawback of both methods is that the measurements are line integrated.

Electrostatic probes are an alternative approach to electron property measurements in HiPIMS plasma. Probe measurements are simple to undertake, but data interpretation is difficult when a magnetic field is present[12,13] and the relative abundance of ionic species is required for calculating ion density (n_i). Previous studies have used target inserts to detect localized ionization zones (spokes) and obtain n_i at the target sheath edge;[14] and (intrusive) Langmuir probes are typically

[a]Electronic mail: ryanp@liverpool.ac.uk

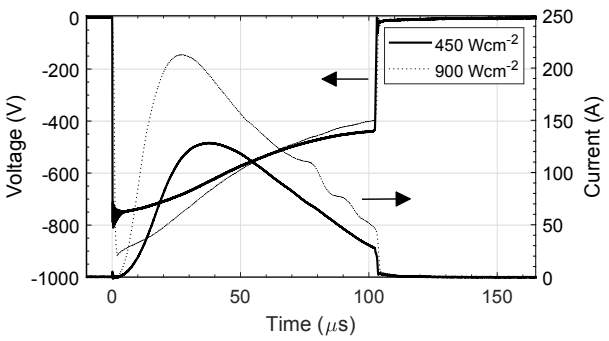

FIG. 2. Current-voltage-time waveforms for the two discharge conditions: peak power densities of 450 Wcm^{-2} and 900 Wcm^{-2} with 12 mTorr of argon gas, pulse width 100 μs and frequency 50 Hz.

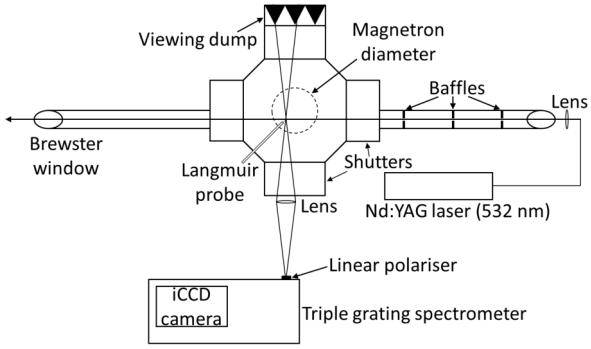

FIG. 3. Schematic of the Thomson scattering apparatus in the magnetic trap measurement configuration. The viewing dump, Brewster windows, baffles and the notch filter in the triple-grating spectrometer attenuate the stray laser light signal reaching the iCCD camera.

used outside of the magnetic trap for measurements of n_i, n_e, T_e and the electron energy distribution function (EEDF).[8,15–17] There have been fewer Langmuir probe studies within the magnetic trap[18,19] because the presence of the probe stem and current drainage to the probe tip are expected to significantly perturb the main ionization region. In addition, data interpretation is simpler far from the target because unmagnetised electron collection by the probe is more valid, and the concern over probe lifetime, due to excessive sputter deposition and melting, is alleviated.

In this letter, we report the first comparison of n_e and T_e measurements in HiPIMS plasma made by Langmuir probe and laser Thomson scattering. The interpretation of the Thomson data is unambiguous and unaffected by magnetic fields and so reliable electron properties can be obtained with excellent spatial ($\lesssim 3$ mm) and temporal resolution (~ 5 μs). The drawback of the technique is that a complex, expensive experimental setup is required which is available in only a few laboratories. The aim of this research is to determine whether a Langmuir probe can provide reliable time-resolved n_e and T_e measurements in HiPIMS plasma, including inside the magnetic trap.

A VTech 150 series unbalanced magnetron (supplied by GENCOA Ltd) equipped with a 150 mm diameter planar tungsten target, was mounted vertically above the vacuum chamber, which was evacuated to a base pressure of $\sim 1 \times 10^{-5}$ Torr. Two different voltage waveforms were applied to the target using a Sinex3 unit (purchased from Chemfilt AB Ltd) with 12 mTorr of argon gas in the chamber. Figure 2 shows the current-voltage-time waveforms and these produced peak power densities of 450 ± 25 Wcm^{-2} and 900 ± 25 Wcm^{-2} (normalised by entire target area). The pulse width and frequency were 100 μs and 50 Hz respectively. The two measurement positions are shown in figure 1.

Laser Thomson scattering is the elastic scattering of laser photons from free electrons in the plasma. In the incoherent limit, the scattering spectrum is proportional to the electron velocity distribution function (EVDF) in one-dimension, so T_e is determined from the spectral width and n_e from the total scattering intensity. A review of laser Thomson scattering applied to low-density glow discharges is given by Muraoka *et al*.[20]

A schematic plan view of the Thomson scattering apparatus is shown in figure 3; the chamber was designed to reduce the amount of stray laser light reaching the detector. A Nd:YAG laser operated at the second-harmonic wavelength 532 nm was the radiation source for the experiment. The laser supplied ~ 230 mJ per pulse at the scattering volume location, had a pulse duration of 5 ns, beam divergence 0.5 mrad and 10 Hz repetition rate. The laser was focused by a 1 m focal length lens so that the beam diameter was ~ 0.25 mm at the measurement position. The beam path was in the plane of the target surface and the laser electric field was linearly polarized in the direction perpendicular to this plane. For the measurements at the magnetic null position, the laser beam passed through the center of the chamber, whereas for the magnetic trap measurements, the beam was offset by 29 mm perpendicular-distance from the center of the chamber. The laser flashlamps were triggered by a TTL signal derived from the HiPIMS voltage waveform.

The scattered light was collected by a lens (75 mm diameter, 200 mm focal length) positioned at 90° with respect to the laser propagation direction. The entrance slit of the spectrometer had an effective aperture 0.30 mm $\times$ 6 mm and its slit height was parallel to the laser propagation direction. A linear polarizer was positioned in-front of the entrance slit to transmit the polarized Thomson photons and attenuate the unpolarized plasma emission signal, thereby improving the signal to noise ratio of the Thomson scattering spectrum. The triple-grating spectrometer was set to the double-subtractive configuration to attenuate the wavelength region 531.5-532.5 nm using a mask for removal of the stray light and Rayleigh signals. An iCCD camera (Andor iStar) recorded the spectra and the measurements were averaged over the spatial dimension. An example Thomson scattering spectrum is shown in figure 4. The wings of the Thomson spectra were fit with either a single or double Gaussian curve (corresponds to a single or bi-Maxwellian EVDF) to obtain n_e and T_e. The system was calibrated using Rayleigh scattering from room temperature argon gas after each Thomson scattering measurement. Frequent calibration was required because the chamber window

transmission decreased as a result of film growth during HiPIMS. The density overestimation due to the changing window transmission was $< 10\%$. The Thomson signal was accumulated from 100 to 600 laser pulses depending on the plasma density and the window transmission.

The Langmuir probe tip consisted of tungsten wire of radius 50 μm and was 'L' shaped. There was ~ 0.25 mm length parallel to the probe stem and 5.5 mm length perpendicular to it. The probe was inserted radially into the vacuum chamber so that the 5.5 mm length was parallel to the target surface-normal. In this orientation, the local magnetic field in the trap (~ 33 mT at the measurement position) is approximately parallel to the probe surface-normal, and so the effect of electron magnetization on the measured probe current-voltage (IV) characteristic is reduced.[21] To acquire the probe IV characteristic, a DC power supply was connected to the probe and manually swept over the range -120 V to 10 V with respect to the chamber ground. Current was calculated by measuring the voltage drop across a high-side sense resistor using the AD8479 precision difference amplifier. The output from the amplifier was averaged over >50 cycles on an oscilloscope which was triggered by the target voltage waveform. Standard probe theory was implemented for electron property measurements:[22] the knee method for n_e using the first derivative to locate the plasma potential and the gradient of the natural logarithm of the electron current ($\ln I_e$) for T_e. I_e was calculated by subtracting the ion current (fit using a function of the form: $A(V_p - V)^{0.5} + B(V_p - V)$ where A and B are fitting coefficients) from the total probe current. Probe n_i was calculated using parameterizations of (orbital-motion) Laframboise (Laf) theory[23] and (radial-motion) ABR-Chen theory.[24] The figures in this letter were produced using the argon ion mass, resulting in lower bounds for n_i, because the relative abundance of argon and tungsten ions was not measured; doubly charged ions have been neglected. The upper bounds calculated using the tungsten mass (not displayed) are a factor 2-3 times larger than the lower bounds. The sum of the square of the residuals was minimised when fitting the theoretical curves to the measured ion current. It should be noted that the probe was not inside the chamber during the Thomson scattering measurements.

Figure 5 shows the temporal profiles of plasma density and T_e at the magnetic null position, where the magnetic field strength is low (< 1 mT), for a peak instantaneous power density of 450 Wcm^{-2}. The time axis begins at the start of the pulse on time, and the activeglow ($0 < t[\mu\text{s}] < 100$) and afterglow ($100 < t[\mu\text{s}] < 20000$) periods are highlighted. The reproducibility of the probe parameters was within 20%. Error bars, representing the standard deviation from multiple measurements, are plotted for some of the Thomson scattering measurements. These results show that the probe generally underestimated the plasma density, but all of the probe theories were within a factor of 2.5 of the Thomson scattering measurements. There was excellent agreement between the diagnostics for T_e measurements except the probe did not observe the cold population of electrons detected by Thomson scattering at $t = 10$ μs (figure 4). The properties of the two electron populations at $t = 10$ μs were $T_e = 0.77 \pm 0.18$ eV and $n_e = (6.74 \pm 1.89) \times 10^{17}$ m^{-3} for the cold group, and $T_e = 3.67 \pm 0.47$ eV and $n_e = (9.95 \pm 1.99) \times 10^{17}$ m^{-3} for the warm group. Generation of a theoretical IV characteristic using the above parameters (not displayed) showed that the IV is dominated by the warm population - the probe measurement system could not resolve the two gradients on the $\ln I_e$ against V plot.

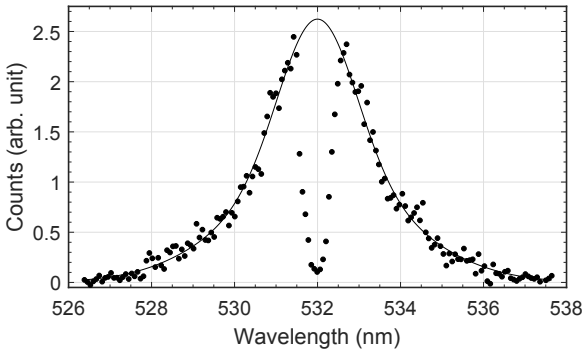

FIG. 4. Thomson scattering spectrum measured at the magnetic null position at $t = 10$ μs with peak power density 450 Wcm^{-2}. A double Gaussian fit was applied to the region outside of the notch filter attenuation (531.5-532.5 nm).

Figure 6 show the diagnostic comparison for density and T_e measurements within the magnetic trap at a peak instantaneous power density of 900 Wcm^{-2}. The probe density theories were within a factor of 2 of the Thomson measurements during the activeglow with the Thomson diagnostic giving a peak density of 6.9×10^{19} m^{-3}. Analysis of the Thomson spectra was consistent with a single Maxwellian EVDF throughout the entire pulse. The probe measurements appeared non-Maxwellian because the only linear region on the $\ln I_e$ against V plot (not displayed) was in the vicinity of the floating potential. This linear region was used to calculate T_e since it is assumed that the collection of the tail of the EEDF is less distorted by the magnetic field due to higher energy electrons having larger gyroradii. The ratio of the probe radius to electron gyroradius, calculated using the Thomson scattering T_e, was between $\sim 0.3 - 0.9$ from $10 \leqslant t[\mu\text{s}] \leqslant 150$, and hence, the effect of electron magnetization on probe collection was important. Nevertheless, there was good T_e agreement between the diagnostics during the activeglow. This indicates that the probe T_e ascribed to the tail of the distribution is representative of the bulk. This justifies the use of triple probes in HiPIMS plasma with similar magnetic field strengths to this study.[19] It should be noted that the plotted afterglow data for the probe is limited (and unreliable) because the IV curves in the vicinity of the floating potential were noisy and the sense resistor value was limited by the maximum current during the voltage pulse. A boxcar method for data acquisition would solve this problem.

We attribute the local minimum in the T_e profiles at $t \sim 50$ μs in figures 5 and 6 to cooling of the EEDF as the density of metallic species in the plasma increased. Following this reduction in T_e, the plasma generation rate and consequently the

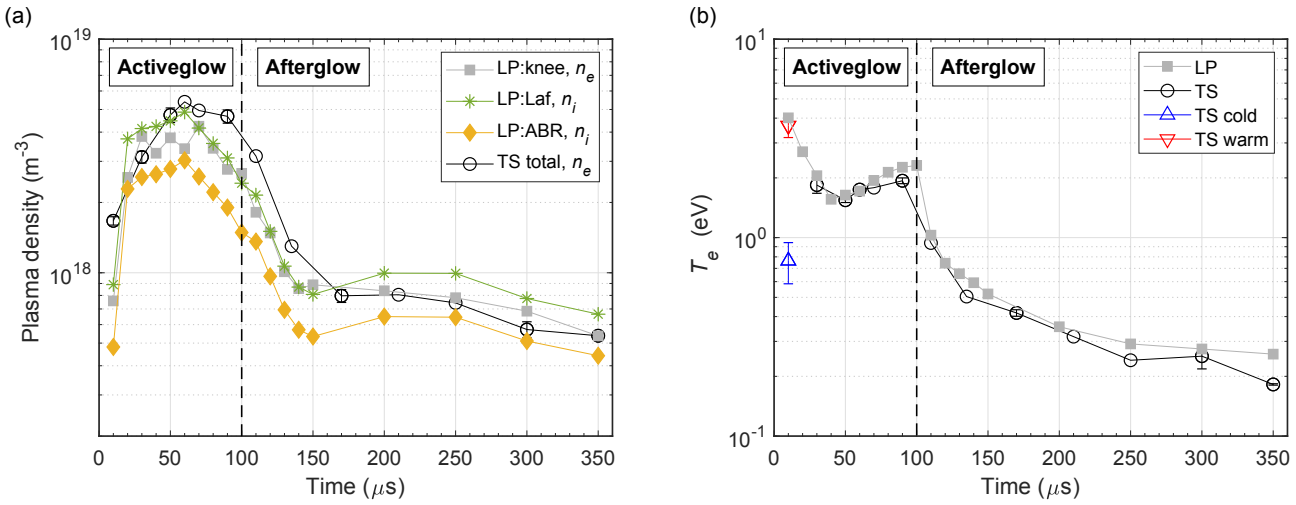

FIG. 5. Temporal profile of plasma density (a) and electron temperature (b) measured by Langmuir probe (LP) and Thomson scattering (TS) at the magnetic null position ($r = 0$ mm, $z = 61$ mm). The three probe densities were determined using the theories indicated in the legend. The T_e values when a double Gaussian fit was applied to the Thomson spectrum are denoted as cold and warm. The argon pressure was 12 mTorr, pulse width 100 μs, pulse frequency 50 Hz and peak power density 450 Wcm^{-2}.

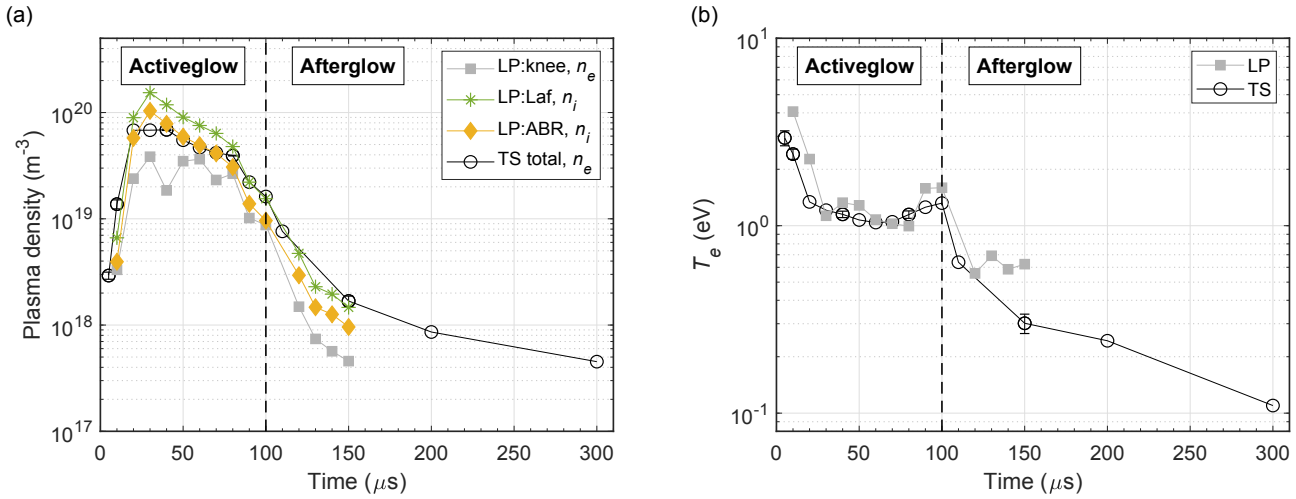

FIG. 6. Temporal profile of plasma density (a) and electron temperature (b) measured by Langmuir probe (LP) and Thomson scattering (TS) within the magnetic trap ($r = 41$ mm, $z = 10$ mm). The three probe densities were determined using the theories indicated in the legend. The argon pressure was 12 mTorr, pulse width 100 μs, pulse frequency 50 Hz and peak power density 900 Wcm^{-2}.

sputtering rate are reduced and so T_e rises. Another interesting feature is the slow plasma density decay in the afterglow. This has been observed in previous studies using probes[15,17,25] and mass spectrometers.[26] The decay of the plasma density was found to proceed according to ambipolar diffusion laws.[25]

In summary, we have reported the first comparison of laser Thomson scattering and Langmuir probes in HiPIMS plasma. Measurements were performed at the magnetic null, where the magnetic field strength is low, and at a position within the magnetic trap. The probe consistently underestimated n_e compared with Thomson scattering, but agreement was generally within a factor of 2, and T_e measurements from both diagnostics were similar. This demonstrates that the Langmuir probe did not significantly perturb the discharge, therefore probes are suitable for measurements of general electron characteristics in HiPIMS plasma. The applicability of a Langmuir probe for investigating highly transient phenomena, such as spokes, remains to be verified. In addition, we were unable to assess the accuracy of the ion collection theories since the ionic species abundance was unknown.

ACKNOWLEDGMENTS

This work was supported by the Engineering and Physical Sciences Research Council [EP/L01663X/1].

[1]U. Helmersson, M. Lattemann, J. Bohlmark, A. P. Ehiasarian, and J. T. Gudmundsson, Thin Solid Films **513**, 1 (2006).

[2]V. Kouznetsov, K. Macák, J. M. Schneider, U. Helmersson, and I. Petrov, Surface and Coatings Technology **122**, 290 (1999).
[3]J. T. Gudmundsson, N. Brenning, D. Lundin, and U. Helmersson, Journal of Vacuum Science & Technology A **30**, 030801 (2012).
[4]M. Samuelsson, D. Lundin, J. Jensen, M. A. Raadu, J. T. Gudmundsson, and U. Helmersson, Surface & Coatings Technology **205**, 591 (2010).
[5]J. Paulitsch, M. Schenkel, T. Zufraß, P. H. Mayrhofer, and W.-D. Münz, Thin Solid Films **518**, 5558 (2010).
[6]F. Magnus, A. S. Ingason, O. B. Sveinsson, S. Olafsson, and J. T. Gudmundsson, Thin Solid Films **520**, 1621 (2011).
[7]J. T. Gudmundsson, Journal of Physics: Conference Series **100**, 082013 (2008).
[8]K. Macák, V. Kouznetsov, J. Schneider, U. Helmersson, and I. Petrov, Journal of Vacuum Science & Technology A **18**, 1533 (2000).
[9]A. P. Ehiasarian, R. New, W.-D. Münz, L. Hultman, U. Helmersson, and V. Kouznetsov, Vacuum **65**, 147 (2002).
[10]J. Bohlmark, J. Alami, C. Christou, A. P. Ehiasarian, and U. Helmersson, Journal of Vacuum Science & Technology A **23**, 18 (2005).
[11]S. M. Meier, A. Hecimovic, T. V. Tsankov, D. Luggenhölscher, and U. Czarnetzki, Plasma Sources Science and Technology **27**, 035006 (2018).
[12]P. C. Stangeby, Plasma Physics and Controlled Fusion **37**, 1337 (1995).
[13]E. Passoth, P. Kudrna, C. Csambal, J. F. Behnke, M. Tichý, and V. Helbig, Journal of Physics D: Applied Physics **30**, 1763 (1997).
[14]A. Hecimovic, J. Held, V. Schulz-von der Gathen, W. Breilmann, C. Maszl, and A. von Keudell, Journal of Physics D: Applied Physics **50**, 505204 (2017).
[15]A. Vetushka and A. P. Ehiasarian, Journal of Physics D: Applied Physics **41**, 015204 (2008).
[16]J. T. Gudmundsson, P. Sigurjonsson, P. Larsson, D. Lundin, and U. Helmersson, Journal of Applied Physics **105**, 123302 (2009).
[17]P. Poolcharuansin and J. W. Bradley, Plasma Sources Science and Technology **19**, 025010 (2010).
[18]J. Bohlmark, J. T. Gudmundsson, J. Alami, M. Latteman, and U. Helmersson, IEEE Transactions on Plasma Science **33**, 346 (2005).
[19]F. Lockwood Estrin, S. K. Karkari, and J. W. Bradley, Journal of Physics D: Applied Physics , 295201 (2017).
[20]K. Muraoka, K. Uchino, and M. D. Bowden, Plasma Physics and Controlled Fusion **40**, 1221 (1998).
[21]J. G. Laframboise and J. Rubinstein, The Physics of Fluids **19**, 1900 (1976).
[22]J. D. Swift and M. J. R. Schwar, *Electrical Probes for Plasma Diagnostics* (Iliffe Books LTD, London, 1970).
[23]F. F. Chen, Physics of Plasmas **8**, 3029 (2001).
[24]P. Kudrna and E. Passoth, Contributions to Plasma Physics **37**, 417 (1997).
[25]L. de Poucques, J. C. Imbert, C. Boisse-Laporte, J. Bretagne, M. Ganciu, L. Teulé-Gay, and M. Touzeau, Plasma Sources Science and Technology **15**, 661 (2006).
[26]A. Hecimovic and A. P. Ehiasarian, Journal of Physics D: Applied Physics **42**, 135209 (2009).